3-D QSAR Investigations of the Inhibition of *Leishmania major* Farnesyl Pyrophosphate Synthase by Bisphosphonates

John M. Sanders,[†] Aurora Ortiz Gómez,[‡] Junhong Mao,[†] Gary A. Meints,[†] Erin M. Van Brussel,[†] Agnieszka Burzynska,[§] Pawel Kafarski,[§] Dolores González-Pacanowska,[‡] and Eric Oldfield*,[†,‖]

Department of Chemistry, University of Illinois at Urbana-Champaign, 600 South Mathews Avenue, Urbana, Illinois 61801; López-Neyra Institute of Parasitology and Biomedicine, CSIC, Granada, Spain; Institute of Organic Chemistry, Biochemistry and Biotechnology, Wroclaw University of Technology, Wroclaw, Poland; and Center for Biophysics and Computational Biology, University of Illinois at Urbana-Champaign, 600 South Mathews Avenue, Urbana, Illinois 61801

We report the activities of 62 bisphosphonates as inhibitors of the *Leishmania major* mevalonate/isoprene biosynthesis pathway enzyme, farnesyl pyrophosphate synthase. The compounds investigated exhibit activities (IC$_{50}$ values) ranging from ∼100 nM to ∼80 μM (corresponding to K_i values as low as 10 nM). The most active compounds were found to be zoledronate (whose single-crystal X-ray structure is reported), pyridinyl-ethane-1-hydroxy-1,1-bisphosphonates or picolyl aminomethylene bisphosphonates. However, N-alicyclic amino-methylene bisphosphonates, such as incadronate (*N*-cycloheptyl aminomethylene bisphospho-nate), as well as aliphatic aminomethylene bisphosphonates containing short (n = 4, 5) alkyl chains, were also active, with IC$_{50}$ values in the 200−1700 nM range (corresponding to K_i values of ∼20−170 nM). Bisphosphonates containing longer or multiple (*N,N*-) alkyl substitutions were inactive, as were aromatic species lacking an *o*- or *m*-nitrogen atom in the ring, or possessing multiple halogen substitutions or a *p*-amino group. To put these observations on a more quantitative structural basis, we used three-dimensional quantitative structure−activity relationship techniques: comparative molecular field analysis (CoMFA) and comparative molecular similarity index analysis (CoMSIA), to investigate which structural features correlated with high activity. Training set results (N = 62 compounds) yielded good correlations with each technique (R^2 = 0.87 and 0.88, respectively), and were further validated by using a training/test set approach. Test set results (N = 24 compounds) indicated that IC$_{50}$ values could be predicted within factors of 2.9 and 2.7 for the CoMFA and CoMSIA methods, respectively. The CoMSIA fields indicated that a positive charge in the bisphosphonate side chain and a hydrophobic feature contributed significantly to activity. Overall, these results are of general interest since they represent the first detailed quantitative structure−activity relationship study of the inhibition of an expressed farnesyl pyrophosphate synthase enzyme by bisphosphonate inhibitors and that the activity of these inhibitors can be predicted within about a factor of 3 by using 3D-QSAR techniques.

Introduction

The leishmaniases are a series of diseases caused by *Leishmania* species.[1] The most lethal form is visceral leishmaniasis (also known as Kala Azar), which is caused by *L. donovani*, with untreated cases reaching a ∼90% mortality rate within 6−24 months.[2] Cutaneous and mucocutaneous leishmaniasis are caused primarily by *L. major* and *L. mexicana*, respectively, and cause severe skin lesions. There are approximately 1.5 million cases of leishmaniasis each year and some 350 million individuals are at risk of infection.[1] The drugs which have been used most frequently to treat the leishma-niases are the pentavalent antimonials Pentostam and Glucantime.[3,4] However, these drugs are quite toxic and

in some areas resistance can be as high as 40%.[5] A second line of defense is the use of AmBisome, a less toxic liposomal formulation of amphotericin B[6] which, because of its cost, is not well suited for use in less developed countries. More recently, the drug Miltefosine has been introduced for the treatment of visceral leishmaniasis,[7,8] and there are promising results with long-term fluconazole treatments for *L. major*,[9] but there is still a need for additional, inexpensive, and effective therapies.

In recent work, it has been found that bisphospho-nates of the type currently in use in bone resorption therapy, such as risedronate (Actonel),[10] and in treating hypercalcemia due to malignancy, such as pamidronate (Aredia),[11] have considerable in vitro activity against a variety of trypanosomatid parasites, including *L. dono-vani*, *Trypanosoma cruzi*, and *Trypanosoma brucei*.[12] Moreover, risedronate effected a parasitological cure of visceral leishmaniasis (caused by *L. donovani*), and pamidronate effected a parasitological cure of cutaneous leishmanisis (caused by *L. mexicana*), in Balb/c mice.[13,14]

* To whom correspondence should be addressed. Telephone: 217-333-3374. Fax: 217-244-0997. E-mail: eo@chad.scs.uiuc.edu.
† Department of Chemistry, University of Illinois at Urbana-Champaign.
‡ López-Neyra Institute of Parasitology and Biomedicine.
§ Wroclaw University of Technology.
‖ Center for Biophysics and Computational Biology, University of Illinois at Urbana-Champaign.

The site of action of these drugs has been shown to be the mevalonate/isoprene biosynthesis pathway enzyme farnesyl pyrophosphate (FPP) synthase,[14−19] and some bisphosphonates have been shown to be potent inhibitors of FPP synthase from the trypanosomatids *T. cruzi* and *T. brucei*.[20,21] Here, we describe the activity of a wide variety of bisphosphonates against a recombinant FPP synthase from *L. major*, the organism responsible for cutaneous leishmaniasis in Europe and Asia. We then use three-dimensional quantitative structure−activity relationship (3D-QSAR) techniques to analyze the results and demonstrate that the QSAR models are predictive. These results may help facilitate the development of novel antileishmanial drugs for treatment of cutaneous and other forms of leishmaniasis in both immunocompetent and immunosuppressed[22] individuals and represent the first comprehensive QSAR investigation of the inhibition of any FPP synthase enzyme by bisphosphonates.

Results and Discussion

We investigated the activity of the 62 bisphosphonates shown in Figure 1 in inhibiting the activity of an expressed *L. major* FPP synthase enzyme, or more specifically, the activity of bisphosphonates in inhibiting the condensation of the homoallylic substrate, isopentenyl pyrophosphate (**1**, IPP), with the allylic substrate, geranyl pyrophosphate (**2**, GPP):
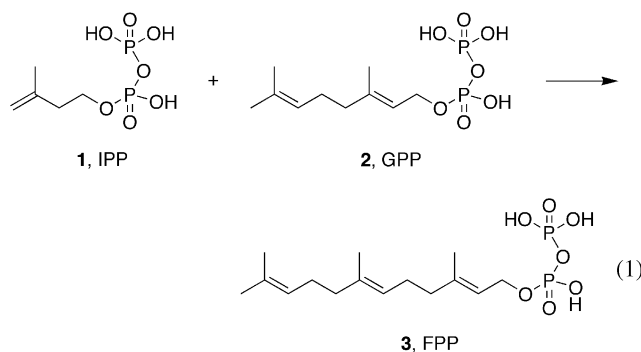
The resulting farnesyl pyrophosphate (**3**, FPP) is used extensively in the biosynthesis of isoprenoids, such as dolichols, in the biosynthesis of sterols, such as ergosterol, as well as in protein prenylation, and is essential for parasite survival. The FPP synthase from *L. major*[23] has a 63% identity with the FPP synthase from *T. brucei*, where RNAi experiments have demonstrated that FPPS is the target for bisphosphonate drugs.[21]

The activities of the compounds investigated (Figure 1) are shown in Table 1 as IC$_{50}$ (μM), K_i (μM) and pIC$_{50}$ (= −log IC$_{50}$ (M)) values, where the IC$_{50}$ values represent the concentrations of bisphosphonates required for 50% enzyme inhibition. Enzyme inhibition was determined basically as described elsewhere for the *T. cruzi* enzyme,[20] by measuring ^{14}C incorporation into FPP from [^{14}C]-IPP (the reaction shown in eq 1). IC$_{50}$ values were obtained from least-squares fits to the following equation:

$$I = \frac{I_{\max} C}{\text{IC}_{50} + C} \quad (2)$$

where *I* is the inhibition fraction, $I_{\max} = 1$, *C* is the

concentration of the inhibitor (μM), and IC$_{50}$ is the concentration (μM) for 50% enzyme inhibition. The K_i values were determined from the relation:[24]

$$K_i = \frac{\text{IC}_{50}}{1 + \dfrac{[\text{GPP}]}{K_m}} \quad (3)$$

where [GPP] = 100 μM and K_m = 10 μM.

Comparative Molecular Field Analysis. To carry out our CoMFA[25] investigations, we basically followed the approaches described previously for investigating the activity of bisphosphonates against the growth of *T. brucei* bloodstream form trypomastigotes,[26] in inhibiting the growth of *Dictyostelium discoideum*, and in bone resorption.[27,28] Bisphosphonate structures were built and then geometry optimized by using a three-step protocol, consisting of steepest-descent, Powell, then BFGS algorithms, using the Tripos force field in the Sybyl 6.9 program.[29] Each energy minimized structure was then aligned to the lowest energy conformation of compound **4** by using the Database Align dialogue in Sybyl 6.9[29] to fit each compound to the (H)O−P−C−P−O(H) atoms in the bisphosphonate backbone common to all of the bisphosphonates investigated. The set of aligned structures is shown in Figure 2. We used default settings to automatically build a 3-D rectangular grid with 2 Å spacing surrounding the alignment shown in Figure 2 and then used hydrophobic, electrostatic, and steric probes to calculate descriptors at these gridpoints. In all cases, we used singly deprotonated phosphonate groups, while the nitrogen-containing side chains were in most cases singly protonated, basically as described before.[26−28] Since the structure and, more particularly, the protonation state of the most active compound, zoledronate (**4**), had not been reported previously, we also carried out a single-crystal X-ray crystallographic study of **4** (crystallized at pH = 7.4) and verified that indeed, the imidazole ring was protonated, as shown in Figure 3. Alkyl chains were constrained to the all-trans geometry. For chiral compounds, the enantiomers which best fit the initial alignment were used in the QSAR calculations. In the cases of compounds **24** and **33**, the chiralities were the same as those used in our previous *T. brucei* QSAR investigation.[26]

We first performed a CoMFA analysis on all 62 compounds using a partial least squares (PLS) approach and a Gasteiger−Marsili charge set.[30] The optimal number of components in the final PLS model was determined to be 6 by using q^2 values, as obtained from the SAMPLS leave-one-out cross-validation technique implemented in Sybyl 6.9.[29] This six component CoMFA model gave a correlation coefficient $R^2 = 0.88$ and a q^2 of 0.50. These and other statistical parameters are given in Table 1, together with the experimental and predicted pIC$_{50}$ values. The training set results for these 62 compounds are shown graphically in Figure 4A.

To validate this CoMFA analysis, we next carried out a series of calculations to evaluate to what extent the CoMFA model had predictive value. To do this, we deleted eight points at random from the training set and computed a new CoMFA model, using this model to predict the activities of the eight excluded compounds. This process was repeated two additional times, giving
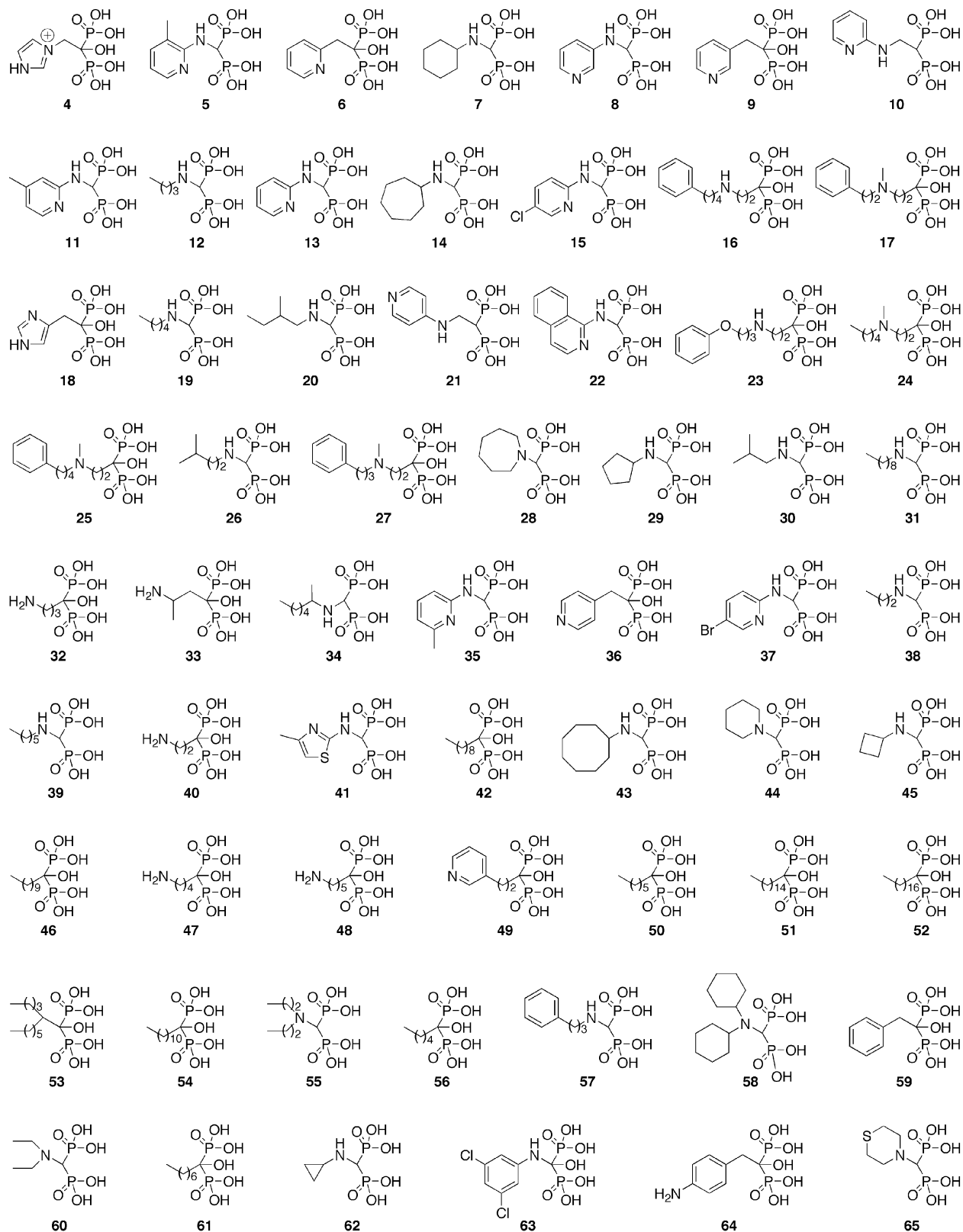
Figure 1. Structures of bisphosphonates investigated, ordered by decreasing activity.

a total of 24 predicted values. The results for the three sets of calculations (24 points) are given in Table 1, in which the predicted values are shown as bold entries, and Figure 4B shows the results of the 24 predictions, graphically. In all cases, the CoMFA models so obtained were statistically significant (Table 1) and the predicted test set values were in generally good agreement with those of the training set, indicating that the training set model is robust with respect to the training set composition. The average pIC_{50} error for the 24 predicted values from the three sets of calculations was 0.44, corresponding to a factor of 2.8 uncertainty in the IC_{50} predictions.

We next used a cross-validation analysis to investigate the stability of the CoMFA analysis with respect to training set composition.[31] The training set model was

Table 1. Experimental (IC$_{50}$, K_i and pIC$_{50}$) and CoMFA Predicted (pIC$_{50}$) Values for Bisphosphonates against *L. major* FPPS and Statistical Results for the CoMFA Models

compound	experimental activity IC$_{50}$ (μM)	K_i (μM)	pIC$_{50}$	predicted pIC$_{50}$[a] Gasteiger−Marsili charges CoMFA training set	CoMFA test set	CoMFA test set	CoMFA test set	predicted pIC$_{50}$[a] MSK charges CoMFA training set	CoMFA test set	CoMFA test set	CoMFA test set
4	0.11	0.010	6.96	6.68	6.72	6.66	6.08	6.69	6.72	6.71	6.15
5	0.11	0.011	6.95	6.74	6.71	**6.41**	6.26	6.79	6.78	**6.44**	6.13
6	0.14	0.014	6.85	6.56	6.67	6.62	6.30	6.39	6.54	6.51	6.25
7	0.16	0.016	6.80	6.47	6.58	6.66	5.91	6.49	6.50	6.67	5.95
8	0.16	0.015	6.80	6.61	6.65	6.67	**6.14**	6.48	6.43	6.54	**5.99**
9	0.17	0.016	6.77	6.70	6.66	6.67	6.36	6.59	6.61	6.61	6.28
10	0.17	0.016	6.77	6.66	6.65	6.75	6.44	6.68	6.71	6.78	6.37
11	0.18	0.017	6.74	6.45	6.47	6.56	6.38	6.56	6.56	6.63	6.27
12	0.21	0.020	6.68	6.20	6.28	6.24	**5.86**	6.24	6.34	6.24	**5.89**
13	0.21	0.020	6.68	6.55	6.50	6.45	**6.37**	6.64	6.58	6.49	**6.25**
14	0.23	0.022	6.64	6.28	6.44	6.64	5.92	6.29	6.36	6.62	5.96
15	0.24	0.023	6.62	6.43	6.38	6.33	6.48	6.50	6.49	6.35	6.36
16	0.25	0.024	6.60	6.67	6.65	6.69	6.54	6.52	6.54	6.64	6.53
17	0.31	0.030	6.51	6.41	6.63	6.46	6.55	6.39	6.50	6.43	6.59
18	0.33	0.032	6.48	6.94	6.82	6.91	6.25	6.87	6.77	6.84	6.27
19	0.35	0.033	6.46	6.03	6.17	6.14	5.95	6.06	6.23	6.15	5.97
20	0.36	0.034	6.44	6.71	6.69	**6.77**	5.93	6.73	6.70	**6.79**	5.96
21	0.42	0.040	6.38	6.20	6.17	6.28	6.33	6.46	6.44	6.52	6.35
22	0.43	0.041	6.37	6.66	6.60	6.61	**6.32**	6.69	6.64	6.66	**6.18**
23	0.45	0.043	6.35	6.35	6.43	**6.46**	6.53	6.27	6.29	**6.50**	6.57
24	0.48	0.046	6.32	6.37	6.44	**6.51**	6.62	6.30	6.32	**6.48**	6.64
25	0.49	0.046	6.31	6.21	6.37	6.17	6.76	6.12	6.14	6.13	6.78
26	0.49	0.047	6.31	6.21	6.27	**6.20**	6.01	6.32	6.41	**6.28**	6.05
27	0.50	0.047	6.31	6.39	6.28	6.38	6.64	6.24	6.21	6.27	6.66
28	0.51	0.049	6.29	5.98	6.19	6.03	5.40	5.91	6.15	6.03	5.40
29	0.54	0.052	6.27	6.24	6.26	6.34	**5.67**	6.26	6.19	6.33	**5.70**
30	0.78	0.075	6.11	6.46	6.35	6.35	5.79	6.45	6.37	6.34	5.83
31	0.90	0.086	6.05	6.28	**6.23**	6.26	6.19	6.15	**6.25**	6.23	6.20
32	0.95	0.091	6.02	6.21	6.10	6.11	6.08	6.27	6.16	6.12	6.08
33	1.0	0.10	5.98	5.89	5.89	5.88	5.76	5.93	5.84	5.89	5.78
34	1.1	0.11	5.94	5.92	5.99	5.87	5.77	5.88	5.87	5.85	5.78
35	1.3	0.12	5.89	5.90	5.92	5.86	6.27	6.09	6.12	6.00	6.23
36	1.3	0.13	5.87	6.42	6.30	6.39	6.36	6.47	6.47	6.50	6.28
37	1.4	0.14	5.85	6.40	6.35	6.31	6.50	6.49	6.47	6.35	6.38
38	1.7	0.16	5.78	6.01	5.98	5.91	5.74	6.03	6.03	5.90	5.76
39	1.7	0.17	**5.76**	5.67	5.76	5.81	5.95	5.69	**5.85**	5.85	5.96
40	1.9	0.18	5.73	5.54	5.51	5.47	5.77	5.46	5.40	5.38	**5.76**
41	1.9	0.18	5.72	5.74	5.69	5.88	5.94	5.65	5.61	5.81	6.00
42	2.4	0.23	5.63	5.30	**5.06**	5.33	5.22	5.34	**5.11**	5.38	5.23
43	2.4	0.23	5.61	6.08	6.22	**6.62**	5.98	6.10	6.19	**6.62**	6.01
44	3.2	0.30	5.49	5.28	5.62	5.26	5.24	5.25	5.64	5.26	5.24
45	3.3	0.31	5.49	5.38	5.35	5.41	5.46	5.35	5.30	5.33	5.48
46	3.4	0.33	5.47	5.42	5.32	5.39	5.25	5.43	5.36	5.42	5.26
47	4.4	0.42	5.36	5.65	5.62	5.63	6.11	5.71	5.70	5.55	6.15
48	4.6	0.44	5.34	5.30	5.27	5.27	6.15	5.36	5.38	5.21	6.21
49	5.4	0.51	5.27	5.31	5.32	5.33	5.70	5.32	5.24	5.33	5.73
50	5.9	0.56	5.23	5.12	5.26	5.27	5.03	5.30	5.35	5.35	5.04
51	6.5	0.62	5.19	5.27	5.01	5.25	5.15	5.18	5.09	5.22	5.16
52	6.7	0.64	5.17	5.26	**5.01**	5.26	5.12	5.16	**5.09**	5.22	5.14
53	6.8	0.65	5.17	5.28	5.31	5.23	4.63	5.16	5.13	5.19	4.59
54	7.8	0.74	5.11	5.31	5.19	5.25	5.21	5.29	5.26	5.24	5.22
55	9.3	0.90	5.03	5.02	4.93	4.92	5.02	4.93	4.97	4.95	5.01
56	9.6	0.92	5.02	5.17	**5.22**	5.25	4.91	5.35	**5.32**	5.32	4.92
57	11	1.0	4.97	4.77	4.65	4.87	5.68	4.85	4.76	4.97	5.70
58	15	1.5	4.82	5.03	**5.71**	4.99	5.20	4.80	**5.63**	5.01	5.21
59	17	1.6	4.78	4.56	4.67	4.55	5.20	4.59	4.63	4.60	**5.20**
60	18	1.7	4.74	4.46	**4.61**	4.40	5.02	4.41	**4.71**	4.41	5.01
61	20	1.9	4.70	4.76	4.83	**4.96**	5.04	4.93	4.93	**5.06**	5.05
62	41	3.9	4.39	4.89	4.70	4.89	5.41	4.85	4.74	4.80	5.46
63	43	4.1	4.37	4.32	4.54	**5.16**	4.88	4.48	4.53	**5.35**	4.79
64	43	4.2	4.36	4.18	4.31	4.12	**5.26**	4.17	4.23	4.14	**5.28**
65	76	7.3	4.12	4.98	**5.40**	4.96	5.16	4.89	**5.46**	4.90	5.15
$R^{2\,b}$				0.88	0.91	0.89	0.59	0.87	0.89	0.89	0.58
$F_{\text{test}}{}^{c}$				64.41	80.64	61.04	36.88	61.02	64.35	60.62	35.40
$q^{2\,d}$				0.50	0.50	0.46	0.40	0.49	0.46	0.46	0.39
N^{e}				6	6	6	2	6	6	6	2
N^{f}				62	54	54	54	62	54	54	54
$q^2{}_{2CV}{}^{g}$				0.41				0.39			
SD (σ) $q^2{}_{2CV}{}^{h}$				0.08				0.09			
$q^2{}_{5CV}{}^{g}$				0.47				0.45			
SD (σ) $q^2{}_{5CV}{}^{h}$				0.05				0.05			
ave. $q^2{}_{random}{}^{i}$				−0.15				−0.16			
max. $q^2{}_{random}{}^{j}$				0.08				0.11			
field contributions steric				0.670	0.666	0.676	0.612	0.666	0.647	0.670	0.631
electrostatic				0.330	0.334	0.324	0.388	0.334	0.353	0.330	0.369

[a] Bold values represent predicted activities of compounds that were not included in the training set. [b] Correlation coefficient. [c] Ratio of R^2 explained to unexplained = $R^2/(1-R^2)$. [d] Cross-validated correlation coefficient after leave-one-out procedure. [e] Optimal number of principal components. [f] Number of compounds. [g] Average cross-validated correlation coefficient for 100 trials using the indicated number of cross-validation groups. [h] Standard deviation of average cross-validated correlation coefficient for 100 trials. [i] Average cross-validated correlation coefficient obtained for random pIC$_{50}$ runs. [j] Maximum cross-validated correlation coefficient obtained for random pIC$_{50}$ runs.
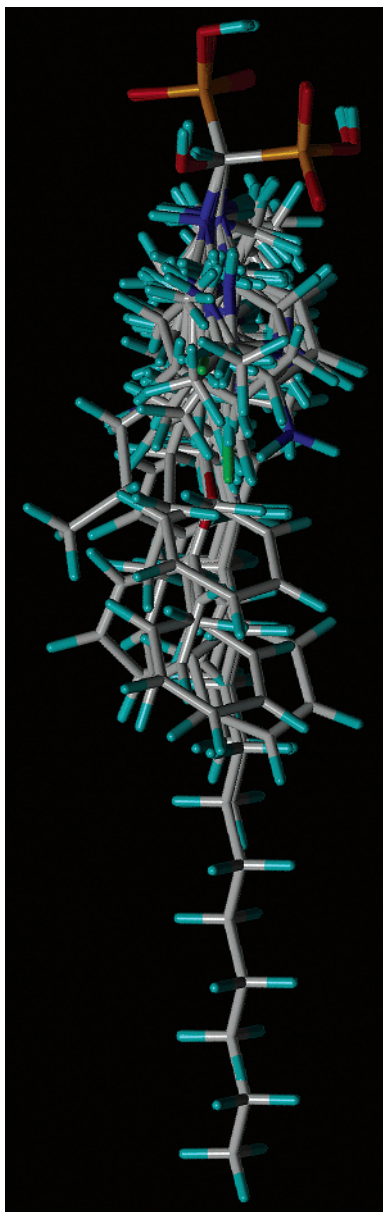
Figure 2. CoMFA (and CoMSIA) structure alignment; superposition of 62 compounds.
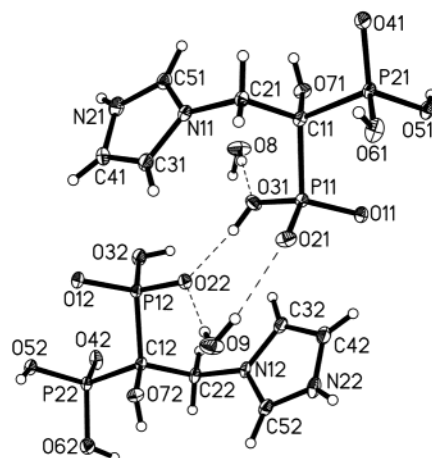

Figure 3. Single-crystal X-ray structures of zoledronate (**4**) crystallized from water. Displacement ellipsoids are drawn at the 35% probability level and H atoms are shown as small spheres of arbitrary radii. Detailed structural information is available in the Supporting Information.

cross-validated using two and five cross-validation groups 100 times each: the average and standard deviation (σ) of q^2 are shown in Table 1. When two cross-validation groups were used, the average q^2 value was 0.41 with $\sigma = 0.08$. The use of two cross-validation groups leaves 31 of the 62 training set molecules in the model construction group and predicts the activities of the remaining 31 compounds. These values were improved, at $q^2 = 0.47$ and $\sigma = 0.05$ with the use of five cross-validation groups, which results in a more consistent cross-validation training set composition for each run.

We also used a random number generator to generate random pIC_{50} values between 4.12 (the activity of the least active compound investigated) and 6.96 (the activity of most active compound investigated). We replaced the experimentally observed pIC_{50} values with the random values and generated new QSAR models using all 62 (random) training set pIC_{50} values. This process was repeated 100 times with the best CoMFA model

yielding a $q^2 = 0.08$ and an average $q^2 < 0$ (Table 1). This suggests that the CoMFA model obtained by using the experimental activities does not result from any chance correlation.

In almost all of the molecules investigated, as noted above, we used protonated side chains since it is thought that N-containing bisphosphonates act as carbocation transition state/reactive intermediate analogues.[32] However, using charged side chains for **63** and **64** gave predicted activities considerably higher than those observed experimentally. This suggested that these species might in fact be nonprotonated. This is consistent with our observation[28] that bisphosphonate activity (in bone resorption) is highly correlated with the pK_a of the parent (heterocycle) base with pK_as in the $\sim$5–9 range being optimum for activity.[28] For **63**, the dichlorosubstitution yields a computed pK_a for the free base of $\sim$2.48 while that for aniline is $\sim$4.61.[33] Thus, **63** is unlikely to be protonated while **64** might be. Likewise, the halogenated species **15** and **37** have pK_a values of $\sim$4.68[33] and might be protonated or nonprotonated. In earlier work,[26] we found that **15** was only a very weak inhibitor of *T. brucei* growth, implying that it is not protonated. To investigate this topic in more detail, we therefore next carried out a single-crystal X-ray crystallographic study of **15**, grown from pH $\sim$5.5 and pH $\sim$2.5 solutions, in addition to exploring the effects of removing **15**, **37**, **63**, and **64** from the training set and using the reduced training set to predict the activities of both protonated and nonprotonated species.

We show in Figure 5 the single-crystal X-ray structures of **15** grown from pH 5.5 (A) and pH 2.5 (B) solutions. At the more basic pH value, we found that the ring was nonprotonated, Figure 5A. This is unprecedented for N-containing bisphosphonates but is consistent with NMR pH titrations of this compound.[34] On the other hand, **15** was found to be ring protonated when crystallized from the more acidic solution, Figure 5B. While the actual protonation state of the bisphosphonates in FPP synthase is clearly not known for certain, these results, together with the observation that
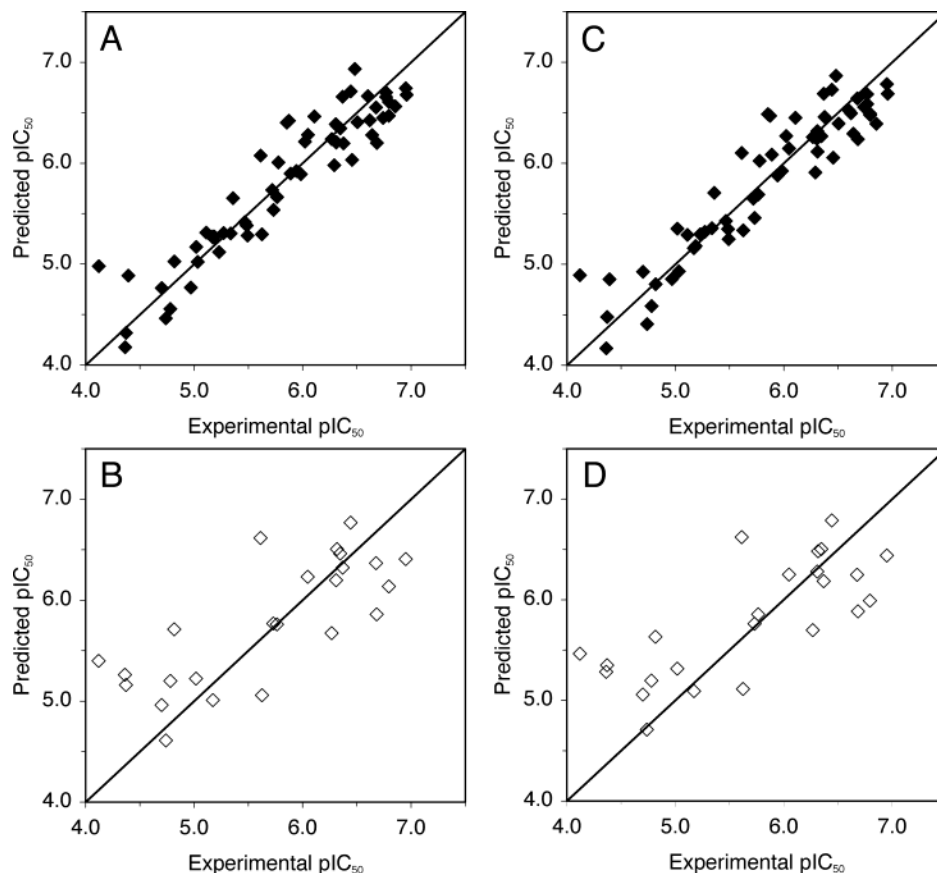
Figure 4. Plots of experimental pIC_{50} versus predicted pIC_{50} values for the CoMFA models of bisphosphonates inhibiting *Leishmania major* FPP synthase. A, 62 compound training set, Gasteiger−Marsili charges; B, results of the three, eight-compound test set prediction studies, Gasteiger−Marsili charges; C, as A but Merz−Singh−Kollman charges; D, as B but MSK charges. The straight lines represent the ideal 45° slopes.

both **15** and **37** have relatively high activity, strongly supports the idea that both bind in their protonated form.

To investigate this question in more detail, we next carried out a series of calculations using a reduced training set of 58 compounds in which **15**, **37**, **63**, and **64** were not included in the set and then predicted the activities of both the protonated and nonprotonated forms of each of these four compounds. Results are shown in Table 2. From Table 2, it can be seen that the nonprotonated nitrogen predictions for **63** and **64** are much closer to experiment than are the protonated nitrogen predictions. For example, the pIC_{50} errors for **63** are 1.20 (charged) and 0.54 (uncharged) while those for **64** are 1.91 (charged) and 0.11 (uncharged), suggesting that the side chains of **63** and **64** bind in an uncharged form to the FPPS enzyme. This is consistent with the weak basicity of anilines and the very weak basicity predicted for the dichloroaniline species, **63**. For the protonated ring form of **15**, the deviation between the experimental pIC_{50} and the predicted pIC_{50} was only 0.16, Table 2, while for the unprotonated form, the error is 1.46. That is, the experimental result can only be reconciled with the predictions by invoking ring protonation in the enzyme. For **37**, the situation is less clear since the computed errors were 0.94 (charged) and 0.78 (uncharged), Table 2. The CoMSIA result however, discussed below, implies that **37** should most likely be treated as a ring protonated species. This clearly illustrates a difficulty with any QSAR analysis in which

the "local pH" value is close to the pK_a value of the compound of interest since both protonated and nonprotonated species, perhaps in exchange, may be present in the experimental sample. Nevertheless, our results do suggest that **15** and **37** are most likely protonated when bound while **63** and **64** are nonprotonated. This lack of activity of bisphosphonates containing weakly basic side chains is also reflected in recent studies on bone resorption[35] in which thiazole-, triazole-, and pyrazole-containing bisphosphonates had little or no activity as bone resorption agents, which can be correlated with parent base pK_a values of <3.[28] On the other hand, the pK_as of aminopyridines and pyridines, the precursors of highly active species such as **5**, **6**, **9**, and **11**, are all in the range 5.52−7.38,[33] and the protonated forms of these species are expected to be good inhibitors, as found experimentally, and as computed using QSAR techniques when using ring-protonated species.

This sensitivity to charge states in several species led us next to consider whether improved results might be obtained by using the Merz−Singh−Kollman (MSK) approach to deduce partial atomic charges,[36] as opposed to our initial use of Gasteiger−Marsili charges.[30] We thus carried out Hartree−Fock calculations using a 6-31G* basis set for each compound using the Gaussian 98 program[37] and used the resulting wave functions to evaluate the MSK charges.[36] The CoMFA test and training set calculations discussed above were then repeated using the MSK charge set. The results are
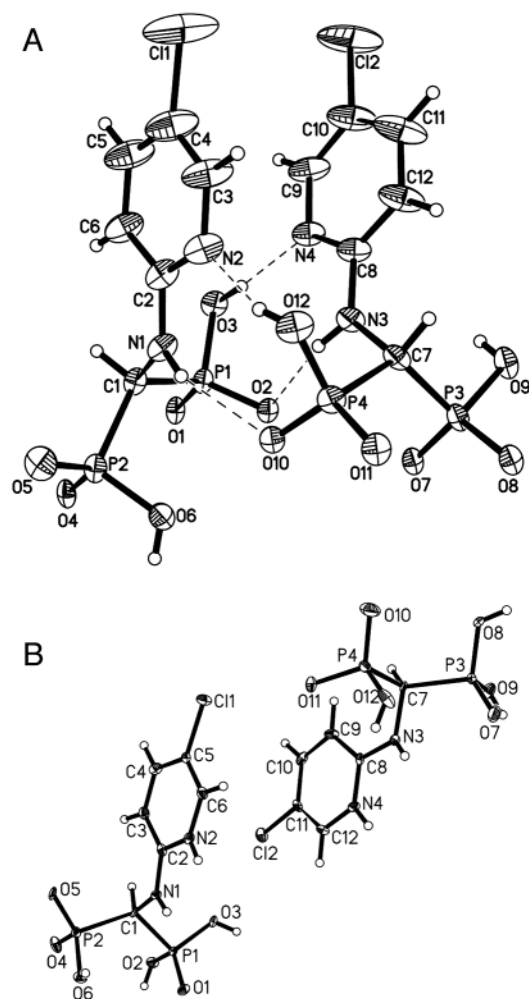
Figure 5. Single-crystal X-ray structures of **15** crystallized at A, pH = 5.5; B, pH = 2.5. Displacement ellipsoids are drawn at the 35% probability level and H atoms are shown as small spheres of arbitrary radii. Detailed structural information is available in the Supporting Information.

Table 2. Experimental and Predicted CoMFA and CoMSIA pIC$_{50}$ Values and Statistical Results of Corresponding Models for Selected Compounds

		predicted pIC$_{50}$ Gasteiger−Marsili charges		predicted pIC$_{50}$ MSK Charges	
compound	exptl pIC$_{50}$	CoMFA pIC$_{50}$	CoMSIA pIC$_{50}$	CoMFA pIC$_{50}$	CoMSIA pIC$_{50}$
15 − charged-N	6.62	6.78	6.28	6.78	6.43
15 − uncharged-N	6.62	5.00	3.99	5.16	4.20
37 − charged-N	5.85	6.77	6.32	6.79	6.46
37 − uncharged-N	5.85	4.90	4.01	5.07	4.24
63 − charged-N	4.37	5.73	5.39	5.57	5.12
63 − uncharged-N	4.37	4.73	4.54	4.91	4.28
64 − charged-N	4.36	5.97	5.53	6.27	5.77
64 − uncharged-N	4.36	4.51	4.27	4.47	4.07
statistics					
R^{2a}		0.88	0.85	0.87	0.88
$F_{\text{test}}{}^{b}$		61.18	46.88	59.18	60.21
q^{2c}		0.45	0.47	0.44	0.55
N^{d}		6	6	6	6
N^{e}		58	58	58	58

[a] Correlation coefficient. [b] Ratio of R^2 explained to unexplained = $R^2/(1 − R^2)$. [c] Cross-validated correlation coefficient after leave-one-out procedure. [d] Optimal number of principal components. [e] Number of compounds.

shown in Tables 1 and 2 and Figures 4C,D but (at least with the CoMFA analysis) are essentially the same, with both yielding about a 67% steric and a 33% contribution to the CoMFA field, Table 1. With the CoMSIA analysis (described below) however, there is a definite improvement when using the ab initio computed charges.

Comparative Molecular Similarity Index Analysis. Next, we investigated the use of the comparative molecular similarity index analysis[38] approach to investigate structure−activity relationships with the bisphosphonates. In contrast to CoMFA, which uses standard Lennard−Jones and Coulombic terms, CoMSIA indices are calculated using Gaussian-type functions. The CoMSIA indices vary less rapidly at short gridpoint-molecule distances than do the CoMFA energies, plus the lattice itself is used to elucidate similarity, and CoMSIA maps are thought by some workers to be more useful since they focus on areas that are actually occupied by ligand atoms.[38] CoMSIA analyses are also typically less sensitive to small alignment errors than are CoMFA analyses, since there are no singularities at ligand atom sites. The CoMSIA analysis was performed basically following the procedure outlined above for the CoMFA analysis and as described in more detail in the Experimental Section. The CoMSIA alignment and grid were the same as those used in the CoMFA analysis discussed above (Figure 2), and the training and test set results are given in Table 3 and graphically in Figure 6A−D. The resulting CoMSIA field maps are shown in Figure 7. **15** and **37** were taken to have protonated rings while **63** and **64** were nonprotonated, in the initial CoMSIA analysis. We also carried out an additional set of calculations in which the activities of these species were predicted using a reduced training set, basically as discussed above. These results are shown in Table 2 and are generally similar to the CoMFA results, with the exception that the CoMSIA analysis with MSK charges more clearly supports the use of a protonated structure for **37**.

For the training set results, we obtain an $R^2 = 0.86$, an F-test value of 54.2, and a q^2 of 0.57 for $N = 62$ compounds using six components, Table 3, using Gasteiger−Marsili charges. The quality of this training set was investigated using two and five cross-validation groups, as described above for the CoMFA analysis. For two cross-validation groups we obtained an average $q^2 = 0.40$ with $\sigma = 0.13$ while with the five cross-validation groups we obtained an average $q^2 = 0.52$ with $\sigma = 0.06$. We also repeated the use of the randomized data analysis discussed above, which also resulted in a negative average q^2 for 100 runs and a maximum q^2 of 0.09 (Table 3), again supporting the validity of the CoMSIA analysis.

As with the CoMFA approach, we also investigated to what extent the CoMSIA method, as applied here to bisphosphonates, is predictive. We again used three 54-compound training sets to predict the activities of three sets of eight compounds. Typical 24 component test set results are shown in Figure 6B. On average, the error in prediction is about a factor of 2.6, slightly better than that obtained with the CoMFA analysis. The training/test set calculations were then repeated using the MSK charge set: results are shown in Table 3 and Figure 6C,D. For CoMSIA, use of the MSK charge set produced slightly improved statistics in all cases (for R^2, F_{test}, q^2, Table 3). The average errors in the CoMSIA test set

Table 3. Experimental (IC$_{50}$, K_i and pIC$_{50}$) and CoMSIA Predicted (pIC$_{50}$) Values for Bisphosphonates against *L. major* FPPS and Statistical Results for the CoMSIA Models

compound	experimental activity IC$_{50}$ (μM)	K_i (μM)	pIC$_{50}$	predicted pIC$_{50}$[a] Gasteiger−Marsili charges CoMSIA training set	CoMSIA test set	CoMSIA test set	CoMSIA test set	predicted pIC$_{50}$[a] MSK charges CoMSIA training set	CoMSIA test set	CoMSIA test set	CoMSIA test set
4	0.11	0.010	6.96	6.62	6.53	6.63	6.75	6.74	6.59	6.77	6.75
5	0.11	0.011	6.95	6.98	6.82	6.84	7.01	6.81	6.74	6.65	6.90
6	0.14	0.014	6.85	6.45	6.68	6.51	6.69	6.53	6.53	6.54	6.70
7	0.16	0.016	6.80	6.40	6.16	6.64	6.33	6.43	6.40	6.66	6.39
8	0.16	0.015	6.80	6.87	6.85	6.96	6.19	6.62	6.62	6.72	5.91
9	0.17	0.016	6.77	6.72	6.87	6.77	6.70	6.61	6.60	6.64	6.49
10	0.17	0.016	6.77	6.79	6.81	6.78	6.64	6.87	6.87	6.92	6.80
11	0.18	0.017	6.74	6.83	6.71	6.85	6.77	6.64	6.59	6.71	6.68
12	0.21	0.020	6.68	6.15	6.18	6.23	6.09	6.26	6.27	6.32	6.19
13	0.21	0.020	6.68	6.77	6.73	6.64	6.61	6.67	6.62	6.57	6.55
14	0.23	0.022	6.64	6.38	6.07	6.77	6.28	6.36	6.31	6.74	6.34
15	0.24	0.023	6.62	6.20	6.19	6.13	6.12	6.09	6.23	6.12	6.22
16	0.25	0.024	6.60	6.56	6.37	6.49	6.61	6.57	6.53	6.59	6.61
17	0.31	0.030	6.51	6.50	6.52	6.51	6.48	6.55	6.58	6.47	6.47
18	0.33	0.032	6.48	6.41	6.56	6.39	6.50	6.58	6.56	6.64	6.48
19	0.35	0.033	6.46	6.02	6.08	6.14	5.95	6.07	6.18	6.16	6.02
20	0.36	0.034	6.44	6.53	6.36	6.63	6.57	6.62	6.51	6.67	6.67
21	0.42	0.040	6.38	6.23	6.00	6.29	6.23	6.31	6.21	6.38	6.49
22	0.43	0.041	6.37	6.81	6.69	6.79	7.11	6.70	6.71	6.66	7.09
23	0.45	0.043	6.35	6.13	6.22	5.96	6.24	6.29	6.22	5.91	6.21
24	0.48	0.046	6.32	6.48	6.36	6.53	6.48	6.45	6.45	6.48	6.44
25	0.49	0.046	6.31	6.31	6.41	6.20	6.31	6.31	6.47	6.12	6.22
26	0.49	0.047	6.31	6.41	6.42	6.53	6.40	6.35	6.46	6.42	6.34
27	0.50	0.047	6.31	6.51	6.36	6.44	6.55	6.45	6.42	6.33	6.42
28	0.51	0.049	6.29	5.79	5.97	5.85	5.86	5.82	6.02	5.79	5.82
29	0.54	0.052	6.27	6.04	5.91	6.19	5.94	6.15	6.12	6.28	6.06
30	0.78	0.075	6.11	6.40	6.31	6.38	6.46	6.45	6.38	6.35	6.48
31	0.90	0.086	6.05	6.09	5.85	6.03	6.09	6.04	6.03	6.06	6.06
32	0.95	0.091	6.02	5.80	5.89	5.88	5.78	5.87	5.71	6.00	5.87
33	1.0	0.10	5.98	5.86	5.87	5.85	5.98	5.81	5.68	5.80	5.87
34	1.1	0.11	5.94	5.81	5.73	5.84	5.80	5.91	5.91	5.91	5.78
35	1.3	0.12	5.89	6.06	6.06	6.04	5.86	5.86	6.03	5.97	5.86
36	1.3	0.13	5.87	6.54	6.69	6.58	6.58	6.64	6.60	6.65	6.57
37	1.4	0.14	5.85	6.18	6.15	6.09	6.10	6.03	6.21	6.06	6.20
38	1.7	0.16	5.78	6.01	6.09	5.97	5.95	6.19	6.18	6.11	6.08
39	1.7	0.17	5.76	5.68	5.75	5.85	5.63	5.75	5.83	5.93	5.73
40	1.9	0.18	5.73	5.56	5.73	5.52	5.67	5.75	5.70	5.72	5.81
41	1.9	0.18	5.72	5.21	5.54	5.32	5.39	5.38	5.42	5.44	5.40
42	2.4	0.23	5.63	5.31	5.11	5.29	5.28	5.29	5.19	5.38	5.32
43	2.4	0.23	5.61	6.37	6.06	6.88	6.31	6.38	6.35	6.89	6.37
44	3.2	0.30	5.49	5.27	5.63	5.29	5.28	5.36	5.66	5.31	5.31
45	3.3	0.31	5.49	5.51	5.62	5.56	5.43	5.59	5.64	5.61	5.45
46	3.4	0.33	5.47	5.45	5.21	5.36	5.42	5.36	5.30	5.40	5.40
47	4.4	0.42	5.36	5.45	5.64	5.45	5.49	5.38	5.17	5.30	5.42
48	4.6	0.44	5.34	5.30	5.63	5.44	5.29	5.41	5.21	5.44	5.36
49	5.4	0.51	5.27	5.15	5.25	5.15	5.16	5.28	5.16	5.25	5.34
50	5.9	0.56	5.23	5.28	5.34	5.38	5.20	5.27	5.30	5.38	5.25
51	6.5	0.62	5.19	5.17	5.26	5.31	5.20	5.15	5.36	5.24	5.16
52	6.7	0.64	5.17	5.11	5.27	5.33	5.16	5.12	5.37	5.24	5.13
53	6.8	0.65	5.17	4.90	4.66	4.81	4.87	4.99	4.96	4.82	4.92
54	7.8	0.74	5.11	5.39	5.20	5.30	5.37	5.29	5.29	5.31	5.32
55	9.3	0.90	5.03	5.10	5.31	5.04	5.14	5.22	5.41	5.07	5.16
56	9.6	0.92	5.02	5.40	5.42	5.46	5.33	5.42	5.36	5.50	5.39
57	11	1.0	4.97	4.87	5.18	4.95	4.98	4.94	5.00	4.98	4.96
58	15	1.5	4.82	4.93	5.25	4.97	5.01	4.88	5.53	4.81	4.83
59	17	1.6	4.78	4.90	5.06	4.88	5.17	4.84	4.82	4.76	5.12
60	18	1.7	4.74	4.70	5.25	4.62	4.74	4.89	5.35	4.75	4.86
61	20	1.9	4.70	4.99	5.05	5.14	4.93	5.00	5.01	5.22	5.00
62	41	3.9	4.39	5.17	5.49	5.17	5.14	4.94	5.13	4.92	4.76
63	43	4.1	4.37	4.41	4.18	5.18	4.09	4.11	4.39	5.00	4.19
64	43	4.2	4.36	4.33	4.24	4.14	4.73	4.16	4.10	4.17	4.71
65	76	7.3	4.12	4.66	5.30	4.69	4.61	4.45	5.20	4.38	4.31
$R^{2 \, b}$				0.86	0.80	0.87	0.86	0.88	0.85	0.90	0.88
$F_{\text{test}}{}^{c}$				54.15	49.19	50.64	46.42	65.69	52.81	67.84	57.76
$R^2_{\text{cv}}{}^{d}$				0.57	0.45	0.51	0.50	0.61	0.50	0.57	0.56
N^{e}				6	4	6	6	6	5	6	6
N^{f}				62	54	54	54	62	54	54	54
$q^2_{\text{2CV}}{}^{g}$				0.40				0.44			
SD (σ) $q^2_{\text{2CV}}{}^{h}$				0.13				0.11			
$q^2_{\text{5CV}}{}^{g}$				0.52				0.57			
SD (σ) $q^2_{\text{5CV}}{}^{h}$				0.06				0.05			
ave. $q^2_{\text{Random}}{}^{i}$				−0.14				−0.14			
max. $q^2_{\text{Random}}{}^{j}$				0.09				0.12			
field contributions											
hydrophobic				0.449	0.422	0.432	0.478	0.418	0.411	0.389	0.450
electrostatic				0.311	0.366	0.323	0.288	0.342	0.350	0.365	0.311
steric				0.240	0.212	0.245	0.234	0.240	0.239	0.246	0.239

[a] Bold values represent predicted activities of compounds that were not included in the training set. [b] Correlation coefficient. [c] Ratio of R^2 explained to unexplained = $R^2/(1-R^2)$. [d] Cross-validated correlation coefficient after leave-one-out procedure. [e] Optimal number of principal components. [f] Number of compounds. [g] Average cross-validated correlation coefficient for 100 trials using the indicated number of cross-validation groups. [h] Standard deviation of average cross-validated correlation coefficient for 100 trials. [i] Average cross-validated correlation coefficient obtained for random pIC$_{50}$ runs. [j] Maximum cross-validated correlation coefficient obtained for random pIC$_{50}$ runs.
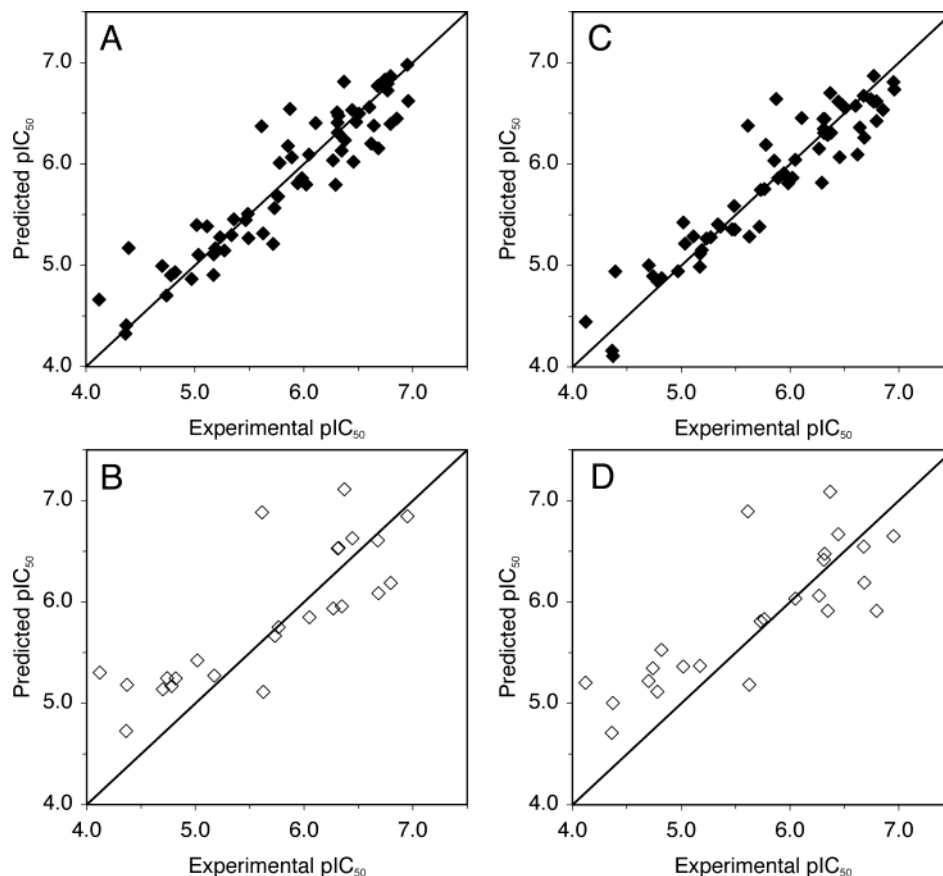
Figure 6. Plots of experimental pIC_{50} versus predicted pIC_{50} values for the CoMSIA models of bisphosphonates inhibiting *Leishmania major* FPP synthase. A, 62 compound training set, Gasteiger charges; B, results of the three, eight-compound test set prediction studies, Gasteiger charges; C, as A but MSK charges; D, as B but MSK charges. The straight lines represent the ideal 45° slopes.

predictions were 0.42 for the Gasteiger−Marsili charge set, 0.43 for the MSK charge set. Overall, a slight improvement over the CoMFA results, Table 1.

The molecular field map results from the training set ($N = 62$) equations are shown in Figure 7. The hydrophobic field contributions are shown in Figure 7A (yellow-favored; white-disfavored) while the electrostatic contributions are shown in Figure 7B (blue-positive charge region; red-negative charge region) and the steric contributions are shown in Figure 7C (green-favored; yellow-disfavored). The individual contributions of each type of descriptor are given in Table 3. The hydrophobic field contributions make the largest contribution (42%) to the overall field and the contour map suggests that enhanced activity might be obtained by further ring substitution. Figure 7B shows a pronounced positive charge field feature (shown in blue), which encompasses the *N*-substituted imidazole feature of **4**, (zoledronate: the most active species; Figure 3). This positive charge feature (blue region) accounts for the high activities of **4**, **5**, **6**, **7**, and **9** (and structurally related compounds) since it almost completely encloses the positive charge region identified in the Merz−Singh−Kollman charge calculations in each of these compounds. Figure 7C shows the steric fields, with the green (attractive) hydrophobic feature clearly encompassing several carbons in the aromatic ring, which can be expected to contribute to the high overall activity of the aryl bisphosphonates versus the alkyl bisphosphonates. With the CoMSIA analysis, we obtained better results by

using hydrophobic, electrostatic, and steric descriptors as opposed to the use of only electrostatic and steric descriptors as in the CoMFA analysis, although the electrostatic contributions were the same in both analyses, contributing ∼1/3 of the overall field.

Activities of Individual Compounds. Finally, we discuss some of the more obvious chemical structure−activity relationships which can be made for the compounds investigated, and make additional correlations with bisphosphonate activity in the literature. Compounds **4**−**32** all have IC_{50} values <1 μM (corresponding to K_i values <100 nM) and are, therefore, quite potent inhibitors of *L. major* FPP synthase. The majority of the most active compounds (**4**, **5**, **6**, **8**, **9**, **10**, **11**) contain both a positive charge feature and an aromatic ring feature, which can presumably help delocalize the charge, although charge delocalization per se is not essential, since this will not occur in other active species, such as **7**, **12**, **14**, and **19**. The actual spatial localization of the positive charge also appears to be relatively flexible (varying from α to γ and δ positions) and presumably reflects a relatively diffuse electrostatic field stabilization by the protein of the putative carbocation. That is, the carbocation is not expected to be stabilized by a specific anionic group (which would likely be reactive), but rather by a more delocalized interaction, such as a cation−π interaction or a more global charge field (electrostatic field) effect. The preferred location of the positive charge feature is clearly identified in the CoMSIA electrostatic fields. Interestingly, some of the
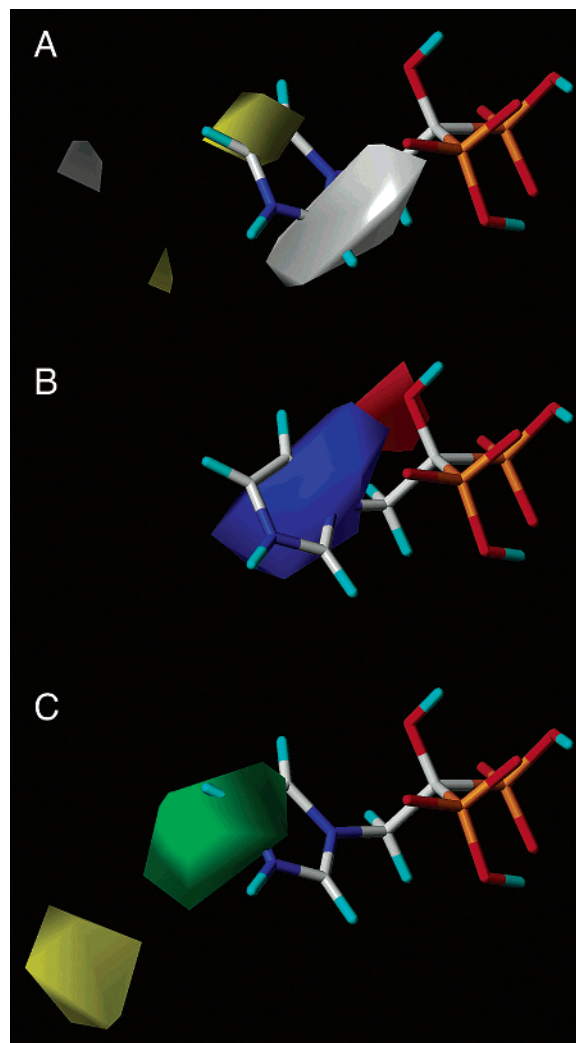
Figure 7. CoMSIA fields for *L. major* FPP synthase inhibition by bisphosphonates. A, Hydrophobic fields. Yellow regions indicate where hydrophobic groups are expected to enhance activity; white regions indicate where hydrophobic groups are expected to reduce activity. B, Electrostatic fields. Blue regions indicate where positive charge is expected to enhance activity; red regions indicate where negative charge is expected to enhance activity. C, Steric fields. Green regions indicate where steric bulk is expected to enhance activity; yellow regions indicate where steric bulk is expected to reduce activity.

general patterns of activity seen in *L. major* FPP synthase inhibition have also been observed in very early patent literature from Nissan where **5**, **11**, **15**, and **35** were identified as herbicides.[39] In that work, the effects of ring substitution were investigated, and it was found that the 3′ (**5**), 4′ (**11**), and 5′ species were highly active, while the 6′ (**35**) and 4′,6′ dimethyl species were very much less active, completely consistent with our observations vs *L. major* FPP synthase. Since Zeneca have shown that **5** is a ∼25 nM inhibitor of a farnesyl pyrophosphate synthase from daffodils,[15] it seems that the herbicidal activity of such bisphosphonates, as well as their antiparasitic[12] and bone resorption activity,[19] may all be attributable to FPP synthase inhibition.

The second set of compounds (**33**−**53**) are less active and have IC$_{50}$ values in the range ∼1−10 μM (Table 1). Eight compounds (**42**, **46**, **50**, **51**, **52**, and **53**) lack a positive charge (nitrogen) feature, which accounts for their lower activity, while five (**32**, **36**, **47**, **48**, **49**) have

the positive charge feature too distal to the bisphosphonate backbone to mimic a GPP carbocation intermediate. Compounds which lack a steric feature (like a ring, as indicated by the green region in Figure 7C), are expected to have lower activity than species where this feature is present. The inactivity of **49**, which has both a carbon ring feature and a positive charge feature, is expected, since the positive charge feature is ϵ to the bisphosphonate backbone[19] and falls outside the region identified by the CoMSIA electrostatic field (Figure 7B). However, this does not mean that bisphosphonates containing ϵ nitrogens will always be inactive. For example, in the context of aminomethylene bisphosphonates, the *p*-pyridyl bisphosphonate (**66**) shown below:

66
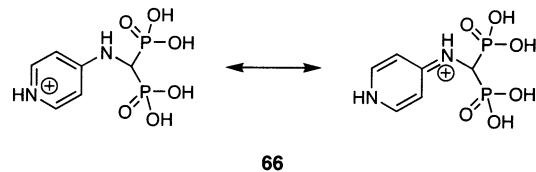
has been shown to be extremely active as an herbicide,[39] most likely due to the possibility of strong quinonoid resonance stabilization which delocalizes the positive charge (as in the amidinium-like species **5**, **8**, **10**, etc.). Similarly, **21** is also capable of this type of resonance stabilization and is quite active in our assay. Notably, while a meta nitrogen does not enable either an amidinium or quinonoid-like resonance stabilization, species such as risedronate (**9**) are of course very active, perhaps due to the positive charge feature being "ideally" located for interaction with the protein. The presence of a polar functionality at the para position, e.g. in the following *para*-methoxy, *p*-hydroxy and *p*-nitro species (**67**−**69**):

67   **68**

69
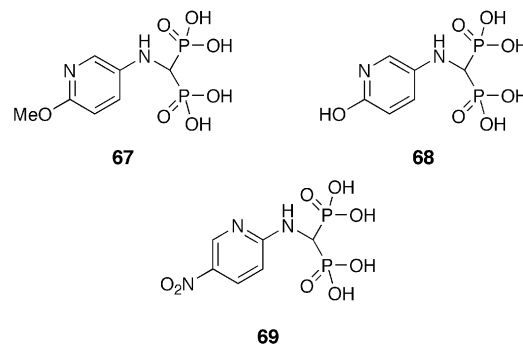
removes essentially all herbicidal activity,[39] consistent with our observation that the *p*-amino species (**64**) has low activity vs *L. major* FPP synthase. The origins of the lower activities of **35** (versus e.g. **5** or **11**) and **37** (versus **15**) suggest a steric effect may also be operative in both compounds. A purely electronic effect of Br in **37** on the pK_a of the nitrogen seems unlikely since the Cl in **15** is expected to be a better electron-withdrawing group. Consequently, it appears likely that there may be steric crowding contributing to the decreasing activity seen on moving from **5** (3′ ring position), to **11** (4′ ring position), to **15** and **37** (5′ ring position) and finally to **35** (6′ ring position). This is consistent with the steric and hydrophobic field results shown in Figure 7 and, indeed, ring methylation in compounds **70** and **71** has been shown to contribute a factor of 100 to inactivity,[19] clearly indicating that a single methyl group can have

70   **71**
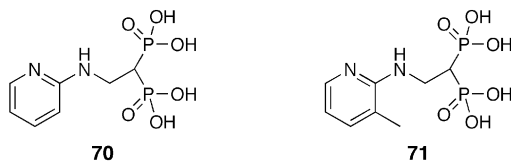
a large repulsive interaction. The activity of **22** is to be expected, since the additional carbons are in the 3′,4′ positions of the pyridine ring, where methylations do not compromise activity, consistent with the favorable hydrophobic field result shown in Figure 7A.

The least active compounds (**54**–**64**) have IC$_{50}$ values in the ~11–76 μM range (Table 1). **59** lacks the positive charge feature, **60** lacks the ring or aliphatic carbon feature, **61** lacks the positive charge feature, and **64** has a ζ-N, distal from the bisphosphonate backbone. In addition, as noted above, the theoretical results suggest that **63** and **64** are not very basic. While these comments are clearly only descriptive, they do give a potentially useful qualitative description of the key features which contribute to bisphosphonate activity and help put the quantitative CoMFA and CoMSIA modeling approaches on a perhaps more readily understood structural basis, which should facilitate future drug design.

Conclusions

The results we have described above are of interest for a number of reasons. First, we have made the first detailed investigation of the inhibition of a recombinant farnesyl pyrophosphate synthase enzyme by 62 1-hydroxy-1,1-bisphosphonates and aminomethylene bisphosphonates. Second, we have made the first detailed CoMFA and CoMSIA investigations of the inhibition of an expressed farnesyl pyrophosphate synthase by bisphosphonates. The CoMFA and CoMSIA training set results have theory-versus-experiment R^2 correlations of ~0.87 and ~0.88, respectively, with F-test values of ~61 (CoMFA) and ~66 (CoMSIA). The CoMFA and CoMSIA results were validated by using two cross-validation and data randomization techniques. Third, we have used a training/test set approach to predict the activities of 24 test set compounds: pIC$_{50}$ errors were ~0.46 (CoMFA) and ~0.43 (CoMSIA), corresponding to average prediction errors of ~2.9 and ~2.7. Fourth, we report CoMSIA field maps which help describe some of the key features of the bisphosphonates important in enzyme inhibition. Fifth, we have provided a descriptive analysis of the activities of the compounds investigated, and made comparisons with the activities of these and other bisphosphonate FPP synthase inhibitors active as herbicides. These comparisons show a number of interesting trends related to ring methyl substitution and activity, the position of ring nitrogens and activity, the likely effects of resonance stabilization, and in some cases the deleterious effects of incorporation of polar substitutions on the aryl rings, which should be of use in the development of other FPP synthase inhibitors.

Experimental Section

Synthetic Aspects. The bisphosphonates investigated were synthesized and characterized basically according to the methods described in refs 12 and 26. In short, 1-hydroxyalkylidene-1,1 bisphosphonates were prepared by reaction of the appropriate carboxylic acid with phosphorous acid and phosphorus trichloride, followed by hydrolysis and in most cases

pH adjustment to 4.3 with a 50% NaOH solution, followed by recrystallization from H$_2$O:[12,26]
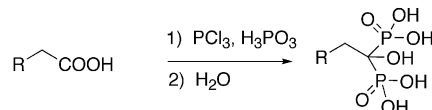
Zoledronate (**4**) was made from the corresponding imidazol-1-ylacetic acid,[40] which was prepared from imidazole using a BBDE Cl[41] phase-transfer catalyst:
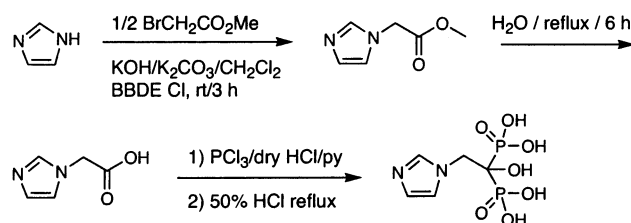
BBDE Cl = 1,5-bis-(*N*-benzyl-*N*,*N*-diethylammonium) diethylether, dichloride

The aminomethylene bisphosphonates were also synthesized basically as described before,[12] by reacting stoichiometric amounts of the corresponding amines, triethyl orthoformate and diethyl phosphite,[12,26] followed by acid hydrolysis, for example:
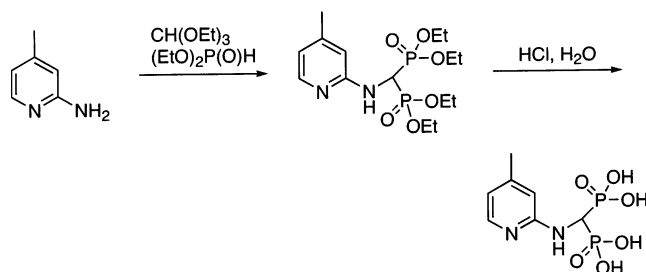
The purity of all samples was verified by microchemical analysis (H/C/N) and in some cases via quantitative ^{1}H NMR spectroscopy. Compounds **5**–**7**, **9**, **11**, **15**, **18**, **19**, **24**, **26**, **32**, **33**, **36**, **37**, **39**, **40**, **42**, **46**–**50**, **54**, **56**, **59**–**61**, and **64** were available from previous work[12,26,42]. All compounds not previously reported, with the exception of the compounds discussed below, had experimental H/C/N analyses that agreed within 0.4% of the calculated values. **4**: Anal. (C$_5$H$_{10}$N$_2$O$_7$P$_2$·H$_2$O) C, H; N: calcd, 9.66; found, 9.25. **13**: Anal. (C$_6$H$_{10}$N$_2$O$_6$P$_2$·0.5H$_2$O) C, N; H: calcd, 4.00; found, 3.56. **17**: Anal. (C$_{12}$H$_{19}$NO$_7$P$_2$Na$_2$·0.5 H$_2$O) C, N; H: calcd, 4.96; found, 5.37. **21**: Anal. (C$_7$H$_{11}$N$_2$O$_7$P$_2$Na) C, N; H: calcd, 3.65; found, 4.19. **22**: Anal. (C$_{10}$H$_{13}$N$_2$O$_6$P$_2$) C, N; H: calcd, 4.11; found, 3.53. **28**: Anal. (C$_7$H$_{17}$NO$_6$P$_2$) H, N; C: calcd, 30.78; found, 30.35. **38**: Anal. (C$_4$H$_{13}$NO$_6$P$_2$·H$_2$O) C, N; H: calcd, 6.02; found, 5.55. **43**: Anal. (C$_9$H$_{21}$NO$_6$P$_2$) H, N; C: calcd, 35.89; found, 35.44. **58**: Anal. (C$_{13}$H$_{27}$NO$_6$P$_2$) C, N; H: calcd, 7.66; found, 8.32. Full analytical data for all compounds not previously reported is provided in the Supporting Information.

Crystallographic Aspects. For zoledronate (**4**), crystals were grown from water in their zwitterionic form. For compound **15**, crystals of the nonprotonated form were obtained by vapor diffusion of ethanol into an aqueous solution (containing Na$^+$, pH = 5.5), while the crystals of the protonated form were grown from water. Single-crystal data were collected on a Siemens (Madison, WI) Platform/CCD diffractometer using the *SHELXTL* system.[43] Five frame series were filtered for statistical outliers then corrected for absorption by integration using *SHELXTL/XPREP*. Crystal structures were solved by direct methods.[44] Donor-H atom positions were refined under restraints to idealized bond distances, with an effective standard deviation of 0.03 Å. The remaining H atoms were included as riding idealized contributors [U_{iso} = 1.2 or 1.5

$U_{eq}(C)$]. The space group choices were confirmed by successful convergence of the full-matrix least-squares refinement on F^2.[44] Final analyses of variance between observed and calculated structure factors showed no dependence on amplitude or resolution. The crystallographic data, space group, and other information related to the crystal structure determination are summarized in the Supporting Information.

***L. major* FPP Synthase Expression.** The coding sequence of the *Leishmania major* farnesyl diphosphate synthase gene was cloned in the expression vector pET11c to give pET*Lm*-FPPS. After induction with 1 mM IPTG for 4 h at 37 °C, FPPS from soluble BL21(DE3)/pET*Lm*FPPS extracts was purified using a combination of ammonium sulfate precipitation and HAP chromatography.

Enzyme Inhibition by Bisphosphonates. Geranyl pyrophosphate and isopentenyl pyrophosphate were from Sigma (St. Louis, MO) and [^{14}C] isopentenyl pyrophosphate (40−60 mCi/mmol) from NEN Life Sciences (Boston, MA). To determine the effects of BPs on FPP synthase activity, drugs were tested at a range of concentrations, from 0.1 to 100 μM. The analyses were carried out in 100 μL reaction mixtures containing 850 nmol of potassium phosphate buffer (pH 7.0), 85 nmol of MgCl$_2$, 10 nmol of geranyl pyrophosphate, and 5 nmol of isopentenyl pyrophosphate (specific activity 6.34 mCi/mmol). The enzyme reaction was initiated by the addition of 10 ng of pure recombinant farnesyl diphosphate synthase, incubated for 15 min at 30 °C and terminated by addition of 1 mL of an aqueous saturated NaCl solution. Radiolabeled FPP was extracted with 1 mL of 1-butanol. After thorough mixing and brief centrifugation, 0.5 mL of the alcohol phase was removed and radioactivity determined by using a scintillation counter. Enzyme inhibition results are expressed as IC$_{50}$ values, which represent the drug concentrations required to reduce enzyme activity by 50%, as pIC$_{50}$ values (= −log IC$_{50}$(M)) and as K_i values and are collected in Table 1.

3D-QSAR/CoMFA/CoMSIA. CoMFA and CoMSIA analyses were performed by using the Sybyl 6.9 program[29] with default settings. Molecular mechanics calculations were performed by using the Tripos force field, with a convergence criterion requiring a minimum RMS gradient of 0.01 kcal/mol·Å at the steepest descent step and an RMS gradient of 0.001 kcal/mol·Å at the Powell and BFGS steps. Structures were optimized to convergence at each minimization step. Atomic charge calculations for CoMFA and CoMSIA analyses were performed on the minimized structures using the Gateiger−Marsili method[30] in Sybyl 6.9 and also by using Hartree−Fock theory with a 6-31G* basis set, by using the Merz−Singh−Kollman method[36] in the Gaussian 98 program.[37] CoMFA energies and CoMSIA indices were calculated on a rectangular grid containing the aligned molecules by using steric and electrostatic probes and hydrophobic, steric and electrostatic probes, respectively. The atomic coordinates of the models were used to compute field values at each point of a 3D grid using a grid spacing of 2.00 Å. To obtain a quantitative analysis of the dependece of enzymatic activity on CoMFA and CoMSIA parameters, PLS analysis was applied, leading to the results shown in Tables 1−3.

Supporting Information Available: Crystallographic data for **4** and **15** (nonprotonated and protonated forms, 19 tables). This information is available free of charge via the Internet at http://pubs.acs.org.

References

(1) http://www.who.int/inf-fs/en/fact116.html. The Leishmaniases and *Leishmania*/HIV Co−Infections. Fact Sheet No. 116. Revised May 2000.

(2) Bora, D. Epidemiology of visceral leishmaniasis in India. *Natl. Med. J. India* **1999**, *12*, 62−68.

(3) Croft, S. L.; Yardley, V. Chemotherapy of leishmaniasis. *Curr. Pharm. Des.* **2002**, *8*, 319−342.

(4) Roberts, W. L.; McMurray, W. J.; Rainey, P. M. Characterization of the antimonial antileishmanial agent meglumine antimonate (Glucantime). *Antimicrob. Agents Chemother.* **1998**, *42*, 1076−1082.

(5) Grogl, M.; Thomason, T. N.; Franke, E. D. Drug resistance in leishmaniasis: its implication in systemic chemotherapy of cutaneous and mucocutaneous disease. *Am. J. Trop. Med. Hyg.* **1992**, *47*, 117−126.

(6) Adler-Moore, J.; Proffitt, R. T. AmBisome: liposomal formulation, structure, mechanism of action and pre-clinical experience. *J. Antimicrob. Chemother.* **2002**, *49*, 21−30.

(7) Unger, C.; Maniera, T.; Kaufmann-Kolle, P.; Eibl, H. In vivo antileishmanial activity of hexadecylphosphocholine and other alkylphosphocholines. *Drugs Today* **1998**, *34*, 133−140.

(8) Escobar, P.; Yardley, V.; Croft, S. L. Activities of hexadecylphosphocholine (Miltefosine), AmBisome, and sodium stibogluconate (Pentostam) against *Leishmania donovani* and immunodeficient scid mice. *Antimicrob. Agents Chemother.* **2001**, *45*, 1872−1875.

(9) Alrajhi, A. A.; Ibrahim, E. A.; De Vol, E. B.; Khairat, M.; Faris, R. M.; Maguire, J. H. Fluconazole for the treatment of cutaneous leishmaniasis caused by *Leishmania major*. *N. Engl. J. Med.* **2002**, *346*, 891−895.

(10) Geusens, P.; McClung, M. Review of risedronate in the treatment of osteoporosis. *Expert Opin. Pharmacother.* **2001**, *2*, 2011−2025.

(11) Pistevou-Gombaki, K.; Eleftheriadis, N.; Sofroniadis, I.; Makris, P.; Kouloulias, V. Palliative treatment of painful bone metastases from non-Hodgkin lymphoma with disodium pamidronate. *J. Exp. Clin. Cancer Res.* **2002**, *21*, 429−432.

(12) Martin, M. B.; Grimley, J. S.; Lewis, J. C.; Heath, H. T. III; Bailey, B. N.; Kendrick, H.; Yardley, V.; Caldera, A.; Lira, R.; Urbina, J. A.; Moreno, S. N.; Docampo, R.; Croft, S. L.; Oldfield, E. Bisphosphonates inhibit the growth of *Trypanosoma brucei*, *Trypanosoma cruzi, Leishmania donovani, Toxoplasma gondii*, and *Plasmodium falciparum*: a potential route to chemotherapy. *J. Med. Chem.* **2001**, *44*, 909−916.

(13) Yardley, V.; Khan, A. A.; Martin, M. B.; Slifer, T. R.; Araujo, F. G.; Moreno, S. N.; Docampo, R.; Croft, S. L.; Oldfield, E. In vivo activities of farnesyl pyrophosphate synthase inhibitors against *Leishmania donovani* and *Toxoplasma gondii*. *Antimicrob. Agents Chemother.* **2002**, *46*, 929−931.

(14) Rodriguez, N.; Bailey, B. N.; Martin, M. B.; Oldfield, E.; Urbina, J. A.; Docampo, R. Radical cure of experimental cutaneous leishmaniasis by the bisphosphonate pamidronate. *J. Infect. Dis.* **2002**, *186*, 138−140.

(15) Cromartie, T. H.; Fisher, K. J.; Grossman, J. N. The discovery of a novel site of action for herbicidal bisphosphonates. *Pesticide Biochem. Physiol.* **1999**, *63*, 114−126.

(16) van Beek, E.; Pieterman, E.; Cohen, L.; Löwik, C.; Papapoulos, S. Farnesyl pyrophosphate synthase is the molecular target of nitrogen-containing bisphosphonates. *Biochem. Biophys. Res. Commun.* **1999**, *264*, 108−111.

(17) Keller, R. K.; Fliesler, S. J. Mechanism of aminobisphosphonate action: characterization of alendronate inhibition of the isoprenoid pathway. *Biochem. Biophys. Res. Commun.* **1999**, *266*, 560−563.

(18) Grove, J. E.; Brown, R. J.; Watts, D. J. The intracellular target for the antiresorptive aminobisphosphonate drugs in *Dictyostelium discoideum* is the enzyme farnesyl diphosphate synthase. *J. Bone Miner. Res.* **2000**, *15*, 971−981.

(19) Dunford, J. E.; Thompson, K.; Coxon, F. P.; Luckman, S. P.; Hahn, F. M.; Poulter, C. D.; Ebetino, F. H.; Rogers, M. J. Structure−activity relationships for inhibition of farnesyl diphosphate synthase in vitro and inhibition of bone resorption in vivo by nitrogen-containing bisphosphonates. *J. Pharmacol. Exp. Ther.* **2001**, *296*, 235−242.

(20) Montalvetti, A.; Bailey, B. N.; Martin, M.; Severin, G.; Oldfield, E.; Docampo, R. Bisphosphonates are potent inhibitors of *Trypanosoma cruzi* farnesyl pyrophosphate synthase. *J. Biol. Chem.* **2001**, *276*, 33930−33937.

(21) Montalvetti, A.; Fernandez, A.; Sanders, J. M.; Ghosh, S.; Van Brussel, E.; Oldfield, E.; Docampo, R. Farnesyl pyrophosphate synthase is an essential enzyme in *Trypanosoma brucei*: in vitro RNA interference and in vivo inhibition studies. *J. Biol. Chem.* **2003**, *278*, 17075−17083.

(22) Rosenthal, E.; Marty, P.; del Giudice, P.; Pradier, C.; Ceppi, C.; Gastaut, J. A.; Le Fichoux, Y.; Cassuto, J. P. HIV and *Leishmania* coinfection: a review of 91 cases with focus on atypical locations of *Leishmania*. *Clin. Infect. Dis.* **2000**, *31*, 1093−1095.

(23) Gómez, A. O.; González-Pacanowska, D., unpublished results.

(24) Cheng, Y.; Prusoff, W. H. Relationship between the inhibition constant (K_I) and the concentration of inhibitor which causes 50% inhibition (I_{50}) of an enzymatic reaction. *Biochem. Pharmacol.* **1973**, *22*, 3099−3108.

(25) Cramer, R. D., III; Patterson, D. E.; Bunce, J. D. Comparative molecular field analysis (CoMFA). 1. Effect of shape on binding of steroids to carrier proteins. *J. Am. Chem. Soc.* **1988**, *110*, 5959−5967.

(26) Martin, M. B.; Sanders, J. M.; Kendrick, H.; de Luca-Fradley, K.; Lewis, J. C.; Grimley, J. S.; Van Brussel, E. M.; Olsen, J. R.; Meints, G. A.; Burzynska, A.; Kafarski, P.; Croft, S. L.; Oldfield, E. Activity of bisphosphonates against *Trypanosoma brucei rhodesiense*. *J. Med. Chem.* **2002**, *45*, 2904−2914.

(27) Szabo, C. M.; Martin, M. B.; Oldfield, E. An investigation of bone resorption and *Dictyostelium discoideum* growth inhibition by bisphosphonate drugs. *J. Med. Chem.* **2002**, *45*, 2894−2903.

(28) Kotsikorou, E.; Oldfield, E. A quantitative structure−activity relationship and pharmacophore modeling investigation of aryl-X and heterocyclic bisphosphonates as bone resorption agents. *J. Med. Chem.* **2003**, *46*, 2932−2944.

(29) SYBYL 6.9, Tripos Inc., 1699 South Hanley Rd., St. Louis, Missouri, 63144.

(30) Gasteiger, J.; Marsili, M. Iterative partial equalization of orbital electronegativity − a rapid access to atomic charges. *Tetrahedron* **1980**, *36*, 3219−3228.

(31) Matter, H.; Kotsonis, P.; Klingler, O.; Strobel, H.; Frohlich, L. G.; Frey, A.; Pfleiderer. W.; Schmidt, H. H. Structural requirements for inhibition of the neuronal nitric oxide synthase (NOS− I): 3D-QSAR analysis of 4-oxo- and 4-amino-pteridine-based inhibitors. *J. Med. Chem.* **2002**, *45*, 2923−2941.

(32) Martin, M. B.; Arnold, W.; Heath, H. T. III; Urbina, J. A.; Oldfield, E. Nitrogen-containing bisphosphonates as carbocation transition state analogues for isoprenoid biosynthesis. *Biochem. Biophys. Res. Commun.* **1999**, *263*, 754−758.

(33) Advanced Chemistry Development (ACD) Software Solaris V4.67.

(34) Matczak-Jon, E.; Sawka-Dobrowolska, W.; Kafarski, P.; Videnova-Adrabinska, V. Molecular organization and solution properties of N-substituted aminomethane-1,1-diphosphonic acids. *New J. Chem.* **2001**, *11*, 1447−1457.

(35) Widler, L.; Jaeggi, K. A.; Glatt, M.; Muller, K.; Bachmann, R.; Bisping, M.; Born, A. R.; Cortesi, R.; Guiglia, G.; Jeker, H.; Klein, R.; Ramseier, U.; Schmid, J.; Schreiber, G.; Seltenmeyer, Y.; Green, J. R. Highly potent geminal bisphosphonates. From pamidronate disodium (Aredia) to zoledronic acid (Zometa). *J. Med. Chem.* **2002**, *45*, 3721−3738.

(36) Besler, B. H.; Merz, K. M.; Kollman, P. A. 1990 Atomic charges derived from semiempirical methods. *J. Comput. Chem.* **1990**, *11*, 431−439.

(37) Frisch, M. J.; Trucks, G. W.; Schlegel, H. B.; Scuseria, G. E.; Robb, M. A.; Cheeseman, J. R.; Zakrzewski, V. G.; Montgomery, J. A., Jr.; Stratmann, R. E.; Burant, J. C.; Dapprich, S.; Millam, J. M.; Daniels, A. D.; Kudin, K. N.; Strain, M. C.; Farkas, O.; Tomasi, J.; Barone, V.; Cossi, M.; Cammi, R.; Mennucci, B.; Pomelli, C.; Adamo, C.; Clifford, S.; Ochterski, J.; Petersson, G. A.; Ayala, P. Y.; Cui, Q.; Morokuma, K.; Malick, D. K.; Rabuck, A. D.; Raghavachari, K.; Foresman, J. B.; Cioslowski, J.; Ortiz, J. V.; Baboul, A. G.; Stefanov, B. B.; Liu, G.; Liashenko, A.; Piskorz, P.; Komaromi, I.; Gomperts, R.; Martin, R. L.; Fox, D. J.; Keith, T.; Al-Laham, M. A.; Peng, C. Y.; Nanayakkara, A.; Challacombe, M.; Gill, P. M. W.; Johnson, B.; Chen, W.; Wong, M. W.; Andres, J. L.; Gonzalez, C.; Head-Gordon, M.; Replogle, E. S.; Pople, J. A. Gaussian 98, Revision A.9, Gaussian, Inc., Pittsburgh, PA, 1998.

(38) Klebe, G.; Abraham, U.; Mietzner, T. Molecular similarity indices in a comparative analysis (CoMSIA) of drug molecules to correlate and predict their biological activity. *J. Med. Chem.* **1994**, *37*, 4130−4146.

(39) Suzuki, F.; Fujikawa, Y.; Yamamoto, S.; Mizutani, H.; Ohya, T.; Ikai, T.; Oguchi, T. N−Pyridylaminomethylene-diphosphonic and compounds. UK Patent Application, 2 004 888 A, 1978.

(40) Gil, S.; Zaderenzo, P.; Cruz, F.; Cerdán, S.; Ballesteros, P. Imidazol-1-ylalkanoic acids as extrinsic 1H NMR probes for the determination of intracellular pH, extracellular pH and cell volume. *Bioorg. Med. Chem.* **1994**, *2*, 305−314.

(41) Alvarez-Builla, J.; Vaquero, J. J.; Garcia Navio, J. L.; Cabello, J. F.; Sunkel, C.; Fau de Casa-Juana, M.; Dorrego, F.; Santos, L. 1,5-bis-(N-benzyl-N, N-dimethylammonium) diethyl ether, dichloride (BBDE Cl). A novel bis-ammonium salt as phase transfer catalyst. *Tetrahedron* **1990**, *46*, 967−978.

(42) Szabo, C. M.; Matsumura, Y.; Fukura, S.; Martin, M. B.; Sanders, J. M.; Sengupta, S.; Cieslak, J. A.; Loftus, T. C.; Lea, C. R.; Lee, H. J.; Koohang, A.; Coates, R. M.; Sagami, H.; Oldfield, E. Inhibition of geranylgeranyl diphosphate synthase by bisphosphonates and diphosphates: a potential route to new bone antiresorption and antiparasitic agents. *J. Med. Chem.* **2002**, *45*, 2185−2196.

(43) Bruker 2001. SMART (Version 5.625), SAINT (Version 6.22) and SHELXTL (Version 6.12). Bruker AXS Inc., Madison, WI.

(44) Sheldrick, G. M. 2001. SHELXL97−2. University of Göttingen, Germany.